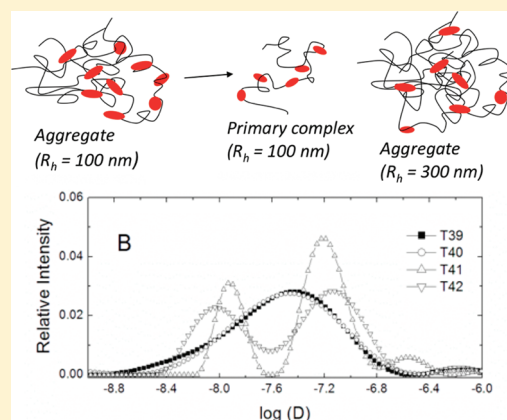


Cluster Formation in Polyelectrolyte–Micelle Complex Coacervation

Ebru Kizilay,[†] Simona Maccarrone,^{†,‡} Elaine Foun,[†] Anthony D. Dinsmore,[‡] and Paul L. Dubin^{*,†}[†]Department of Chemistry and [‡]Department of Physics, University of Massachusetts Amherst, Amherst, Massachusetts 01003, United States

ABSTRACT: The temperature-induced liquid–liquid phase transition (complex coacervation) of a polycation–anionic/nonionic mixed micelle system was examined over a range of macroion concentrations and polycation molecular weights (MW) using turbidimetry and dynamic light scattering (DLS). DLS revealed a progressive increase in complex/aggregate size with temperature up to the phase transition at T_ϕ , followed by splitting of these clusters into respectively smaller and larger particles. We present two explanations: (1) large (200–400 nm) clusters (soluble aggregates) are necessary and sufficient coacervation precursors, and (2) the process of coacervation itself is accompanied by the expulsion of smaller aggregates to form submicrometer droplets. Although a reduction in T_ϕ for higher MW appears to be correlated with larger clusters, in support of model 1, the opposite correlation between cluster size and T_ϕ is seen upon isoionic dilution. We conclude that enhanced coacervation and increased cluster size at high polymer MW arise independently from increased intercomplex attractive forces. Dilution, on the other hand, leads to diminished cluster size, whereas the decrease in T_ϕ on dilution is a reflection of coacervate self-suppression, previously observed for this system. The splitting of clusters into large and small species near T_ϕ is explained by macroion disproportionation, as proposed by Shkolovskii et al for DNA condensation. We demonstrate and explain a similar phenomenon: broadening of the phase transition by an increase in cluster polydispersity, resulting from an increase in surfactant polydispersity.



■ INTRODUCTION

Complex coacervation is a spontaneous liquid/liquid phase separation that occurs when oppositely charged macroions (or polyelectrolytes) are mixed. The process of coacervation leads to the formation of a dense macroion-rich phase (the coacervate) in equilibrium with a dilute macroion-poor phase (continuous phase or supernatant). The principal requirements for such behavior appear to be the formation of soluble complexes with near-neutral charge and noncomplementarity between macroions, including gelatins of different isoelectric points,^{1–3} proteins with either synthetic^{4,5} or natural PEs,^{6,7} PEs with dendrimers,⁸ and PEs with oppositely charged surfactant micelles.⁹ If ion-pairing is too efficient, precipitation will occur. An advantage of the system consisting of PEs with oppositely charged surfactant micelles is that micelle surface charge density (σ , C nm^{−2}) can be varied continuously in a given sample via pH¹⁰ or mixed surfactant stoichiometry.^{11,12} Tuning σ allows construction of phase boundaries, which describe the formation of soluble complexes and coacervates at values of σ that depend on key electrostatic variables, that is, ionic strength, I , and polyelectrolyte linear charge density, ξ . The observed interdependence of σ , I , and ξ facilitate comparison of experiment with theories of polyelectrolyte–colloid interaction^{13,14} and intermacroion condensation.^{15,16}

Coacervation is relevant to such diverse areas as microencapsulation¹⁷ and tissue elasticity¹⁸ with applications in

cosmetic formulations,¹⁹ enzyme immobilization,²⁰ food science,^{21–23} and drug delivery.²⁴ Because of these applications and because of some fascinating biological implications,²⁵ there has recently been a resurgence of interest in coacervation. (The number of papers with coacervation/coacervate in their titles in the last three years surpassed the total published during the preceding decade.) This recent work has expanded our understanding of coacervation beyond the pioneering efforts^{26–28} of a half-century ago, which afforded remarkable insights, given the complexity and limited characterization of the natural polymers then employed and the even more modest instrumentation then at hand. After a decade of quiescence, fundamental understanding has proceeded along three lines: a thermodynamic approach characterized by establishing phase boundaries or diagrams;^{29,30} structural analysis of the coacervate itself;^{31–36} and mechanistic approaches, designed to elucidate the molecular events involved in coacervation including identification of the system at incipient coacervation.³⁷

Complex coacervation might fruitfully be considered from the perspective of colloidal clustering,²² though this idea has not

Special Issue: Clusters in Complex Fluids

Received: October 12, 2010

Revised: February 15, 2011

Published: March 28, 2011

been widespread in part because the field developed from the vantage point of the association of flexible polyampholytes (i.e. gelatin) not viewed as colloidal particles. It is clear—at least for colloid-polyelectrolyte coacervation—that well-defined and thermodynamically stable intermacroionic aggregates exist near the point of phase separation and that repulsive and attractive interactions among them play a role in their coalescence. These clusters possess structural hierarchies far more subtle than conventional colloids: at the largest scale, multipolymer aggregates arise from the association of intrapolymer complexes, which in turn arise from the binding to polymers of micelles, which themselves are surfactant aggregates. The primarily electrostatic repulsive and attractive forces operating over different length scales determine the cluster sizes and structures of the resulting dense phases. The possible retention of aggregate structural features within the macroscopically homogeneous dense phase, an interesting question that has yet to be resolved, will not be dealt with here. In the present work, we consider how the length scales seen in precoacervate clusters (i.e., in single-phase samples near the phase separation point) arise from charge neutrality.

Charge neutralization, which plays a central role in coacervation, refers both to bulk charge stoichiometry of the macroions and to microscopic stoichiometry of the spontaneously formed intermacroion complexes. At the macroscopic level, we define the bulk charge stoichiometry as $X = [+]/[-]$, where $[+]$ and $[-]$ are the concentrations of uncompensated charges on the added macroions (polyelectrolytes, micelles, particles, etc.) in the mixture. At the microscopic or mesoscopic scale, we define a charge stoichiometry coming from the intermacroion complexes: ($x = Z_+/Z_-$), where this ratio depends on the contents of the complexes themselves, not including accompanying counterions. Although X and x are precisely equal only in the absence of free macroions, their proximity is attested to by maximal phase separation when the former is near unity. This condition, and hence, the two-phase state, can be approached by changing the weight mixing ratio or by altering the molecular charge of one macroion, most commonly by pH adjustment, or by increasing the intermacroion binding affinity; for example, by reduction of ionic strength.^{38,39} There have been relatively few systematic studies of the evolution of species in the one-phase region as the two-phase region is approached, due in part to the difficulty of eliminating kinetic effects when coacervation is attained by a mixing process. Polyelectrolyte–micelle systems appear to display rather unique thermally induced coacervation at an experimentally well-defined temperature, T_ϕ . This temperature, T_ϕ , depends on mixed micelle charge, ionic strength, polymer MW, and X , the last being controlled by the ratio of total surfactant/polymer along with the ratio of ionic/nonionic surfactants.³⁷ It can therefore be adjusted for convenience of study.

Our interest is the evolution of the structure of soluble complexes and clusters thereof as the two-phase region is approached under conditions of varying polymer molecular weight and concentration. We examine the phase behavior of a polycation–anionic/nonionic mixed micelle system—poly-(dimethyldiallylammonium chloride)/sodium dodecylsulfate–Triton X-100—over a wide range of surfactant compositions, ionic strengths, and polycation molecular weights using turbidimetry and dynamic light scattering. We focus on the minimal requirements for soluble aggregates at the state of incipient coacervation (i.e., in the single-phase region, but close to the phase-separation point). Somewhat surprisingly, we do not find a simple correlation between T_ϕ and the size of the soluble

aggregates at incipient coacervation. This behavior may in part be explained by the ability of soluble aggregates to undergo spontaneous disproportionation in a manner described by Shklovskii's zeroth-order model for DNA–spermine condensation.⁴⁰

Complex coacervation might also be considered from the perspective of colloidal clustering. The competition between short-range attraction and longer-range repulsion (SALR) operating over different length scales determine the cluster sizes and structures of the resulting dense phases.^{41–46} Colloidal systems interacting via SALR possess a rich phase behavior and may exhibit one or more stable liquid–liquid phase transitions.^{47,48} The effect of the repulsion has been found to be analogous to the liquid–vapor critical point and a portion of the associated liquid–vapor transition line, with two first-order phase transitions: one from the vapor to a fluid of spherical liquid-like clusters and the other from the liquid to a fluid of spherical voids.⁸

Those concepts can be applied to the case of polyelectrolyte–micelle complexation and coacervation, where the long-range electrostatic repulsions among complexes of like charge, subject to screening, compete with short-range attractions between complexes due to polarization or disproportionation. Temperature is the parameter that ameliorates the Coulomb repulsion among polyelectrolyte complexes, by promoting the entropy of counterion expulsion, as clustering or phase separation of complexes leads to the replacement of macroion-bound counterions by intermacroionic ion-pairing. This *colloidal* model in which the polyelectrolyte–micelle complexes are viewed as intricately hierarchical soft colloidal particles, would then predict the coexistence of supernatant droplets (voids) in a coacervate dense medium at high volume fractions with coacervate droplets (liquidlike clusters on micrometer or submicrometer scale) in the supernatant at low volume fraction. This scenario implies the retention of micelle–polyelectrolyte aggregate structural features within the macroscopically homogeneous dense phase that finds only limited experimental evidence so far.^{49–51} In the present work, we consider how the length scales seen in precoacervate clusters (i.e., in single-phase samples near the phase separation point) arise from the tendency toward charge neutrality as the system strives for charge complementarity and counterion release. The polyelectrolyte/surfactant micelle system chosen (PDADMAC/SDS-TX100), extensively studied in our prior work, offers several advantages: (a) the micelle surface charge density can be controlled by the ratio of anionic/nonionic surfactant, (b) the availability of TX100 analogs of varying chemical monodispersity allow us to examine this parameter, and (c) PDADMAC (a “strong”—pH-independent—polycation) appears to have charge spacing especially well-suited for coacervate formation and is used here in the form of well-characterized samples whose narrow molecular weight distributions limit the broadening of transitions due to polydispersity.

■ EXPERIMENTAL SECTION

Materials. Poly(diallyldimethylammonium chloride) (PDADMAC) was prepared by free radical aqueous polymerization of diallylmethylammonium chloride and characterized by light scattering and osmometry.⁵² The two PDADMAC samples will be referred to according to their number average molecular weights (from membrane osmometry) $M_n = 2.7 \times 10^5$, 9.8×10^4 , 1.4×10^5 , and 4.6×10^5 . Triton X-100 (TX100)

and sodium dodecyl sulfate (SDS, purity >99%) were purchased from Aldrich, and NaCl was from Fisher. Monodisperse hexaoxyethylene dodecyl ether ($C_{12}E_8$) was from Nikkol Chemical Co. (Tokyo), and a commercial sample with head-group polydispersity was a gift from Shiseido Corp. (Yokohama, Japan). All were used without further purification. Milli-Q water was used in all experiments.

To bring the systems to the state of soluble complexes, 60 mM SDS in 0.40 M NaCl was added with continuous stirring to solutions of 5 g/L PDADMAC in 33.3 mM TX100 or to 3 g/L PDADMAC in 20 mM TX100, also in 0.4 M NaCl, to bring the mole fraction of SDS (Y) to 0.30. Y is defined as

$$Y = \frac{[\text{SDS}]}{[\text{SDS}] + [\text{TX100}]} \quad (1)$$

which is proportional to the average mixed micelle surface charge density σ . At ionic strength of 0.40 M, the critical micelle surface charge density at the onset of micelle–polycation complex formation, corresponds to $Y_c = 0.23$; at lower values of Y , no micelle–PE interactions take place.⁹ Although $Y = 0.30$ is sufficient for complex formation, the number of micelles bound is insufficient for charge neutralization, and complexes are net positive.^{9,12}

Isoionic dilutions of solutions 5 g/L in PDADMAC were carried out so as to maintain a constant Y , constant polymer/surfactant stoichiometry, and constant ionic strength.

Turbidimetric Measurements. Turbidity, reported as 100 – %T ($\pm 0.1\%$ T), was measured using a Brinkmann PC 800 colorimeter ($\lambda = 450$ nm) equipped with a 1.0 cm path length fiber-optics probe. Turbidity values were recorded as function of temperature with the sample continuously stirred during the heating. Sample temperatures rose at a rate of ~ 1 °C/min. All measured values were corrected by subtracting the turbidity of a polymer-free blank. Duplicate titrations gave reproducible results.

Dynamic Light Scattering (DLS). DLS measurements were carried out with (1) an ALV instrument equipped with a model 5000 Multitau digital correlator and employing a 3 W Ar ion laser source operating at 514 nm at scattering angle 90° at temperatures from 25 to 42 ± 0.5 °C, and (2) a Malvern Instruments Zetasizer Nanosystem at scattering angle 173° at temperatures from 5 to 47 ± 0.5 °C.

The samples were stirred at least 2 h before measurements and filtered with Whatman (0.2 μm) filters prior to measurements. The correlation functions of the scattering data were analyzed via the method of regularization (CONTIN)⁵³ and then used to determine the diffusion coefficients (D). The diffusion coefficient D can be converted into hydrodynamic radii using the Stokes–Einstein equation:

$$R_H = \frac{kT}{6\pi\eta D} \quad (2)$$

where k is the Boltzmann constant, T is the absolute temperature, and η is the solvent viscosity, here taken as that of water.

Measurement of Coacervate Yield. Samples were centrifuged according to ref 37 to yield an upper dilute phase (supernatant) and lower viscous optically clear dense phase (coacervate). The volume of coacervate was recorded. The supernatant was removed and brought to the next temperature, and the process was repeated until no further coacervate could be obtained.

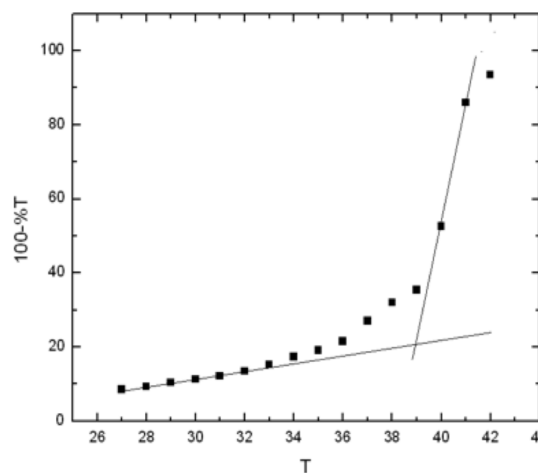


Figure 1. Turbidity as a function of temperature for PDADMAC/TX100-SDS solution. $C_p = 3$ g/L; $M_n = 2.7 \times 10^5$; $Y = 0.30$. Lines drawn to indicate definition of T_ϕ .

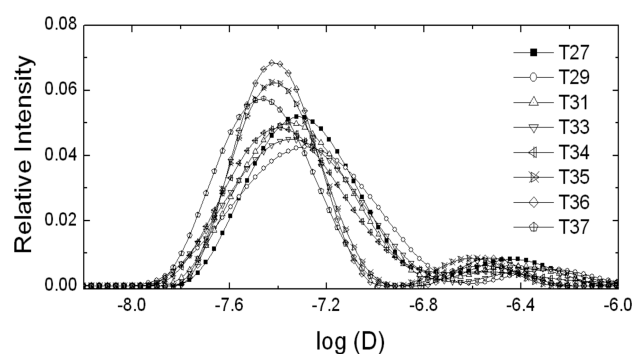


Figure 2. Relative intensity versus diffusion coefficient for PDADMAC/TX100-SDS at temperatures shown (for the sample used in Figure 1). Only free micelles and complexes can be detected.

RESULT AND DISCUSSION

Clustering and Splitting of Complex Aggregates. The onset of coacervation is manifested by an increase in turbidity, as shown in Figure 1. Although this does not appear as a sharp transition, it is nevertheless useful to refer to the discontinuity as T_ϕ , operationally defined by the intersection of the two lines shown.³⁷ This discontinuity corresponds to a liquid–liquid phase separation (coacervation), inasmuch as centrifugation at $T > T_\phi = 39 \pm 1$ °C (4700 rpm, 60 min) results in separation of optically clear dense and dilute phases,^{35,32} the dense phase first appearing as 500–600 nm droplets.³⁷ The nature of species formed at $T < T_\phi$ was examined by DLS; the results are in Figure 2. The results below 34 °C are consistent with radii of intrapolymer complexes.⁵⁴ Comparison of Figures 1 and 2 shows that the change in turbidity commencing at 35 °C coincides with a shift of the slow mode to lower D , corresponding to cluster sizes of 100 nm,³⁷ which suggests interpolymer complexation. Subsequent broadening in the distribution occurring at 39 and 40 °C corresponds mainly to extension to aggregate sizes above 100 nm. The progressive increase in complex size with temperature up to this point changes dramatically above 40 °C as the system splits into two components with apparent radii of 300 and 35 nm. The DLS results are stable at temperatures at or below

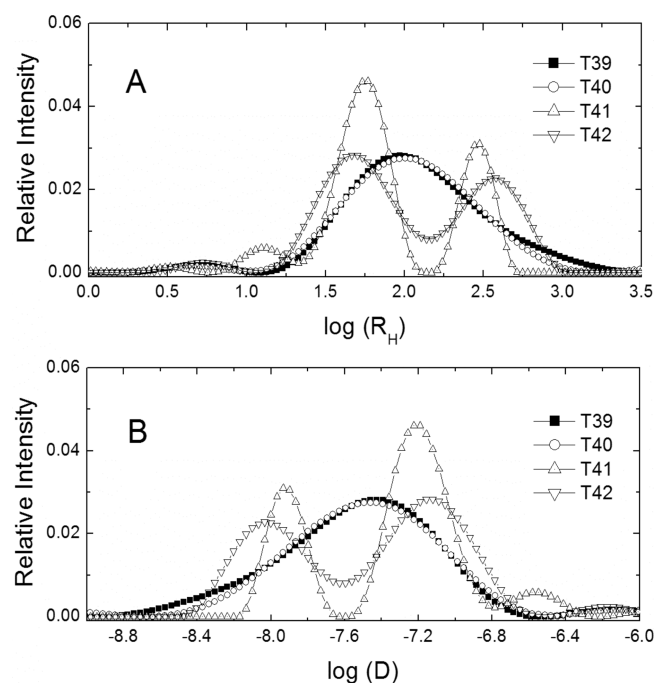


Figure 3. Relative intensity vs (A) hydrodynamic radius (R_H) and (B) diffusion coefficient for PDADMAC/TX100-SDS from 39 to 42 °C. For 39 and 40 °C, the broadening of the apparent distribution is qualitatively different from lower temperatures, extending to diffusivities $<10^{-9}$, corresponding to droplets >400 nm, which form above $T_\phi = 39 \pm 1$ °C (see Figure 1), but do not sediment at ambient conditions.

39 °C, whereas for $T > 42$ °C, the system changes over time as the phase separation occurs.

It appears that the formation of large (~ 300 nm radius) soluble aggregates, coexisting with 35 nm complexes, precedes coacervation, which occurs at $T > 42$ °C. Since only the smaller of these two species remains in the supernatant after gradual deposition of the dense phase, the larger can be identified as either a soluble aggregate susceptible to coacervation or small droplets of the coacervate itself, although its time independence appears to suggest the former. In the first case, we might consider that the forces responsible for the formation of large aggregates subsequently lead to coacervation (in other words, the larger aggregates are literally precursors of coacervation and grow as T is approached); in the latter case, we might consider that the very process of coacervation goes hand-in-hand with the expulsion of the smaller aggregates from the coacervate. The former scenario suggests that complex size might be prerequisite to coacervation and might correlate with incipient coacervation. DLS results are stable at temperatures at 39 °C, in contrast to $T > 42$ °C, but this does not remove ambiguity from the important results at 40 and 41 °C.

Regardless of whether splitting is a cause or effect of disproportionation, it appears that the formation of large (here, ~ 300 nm radius), soluble aggregates precedes coacervation. To examine the effect of aggregate size on coacervation, we varied the polymer MW from 270 kDa to 98 kDa, with the result shown in Figure 4. The size of soluble aggregates varies from 30 to 100 nm for PDADMAC $M_n = 98$ kDa, and from 60 to 180 nm for $M_n = 270$ kDa. If the size of the complex were simply proportional to the size of the polymer, we could write $R_2/R_1 = (M_2/M_1)^{(1+a)/3}$ where a is the Mark–Houwink exponent for the polymer–micelle complex. At 25 °C, we obtain from Figure 4b,

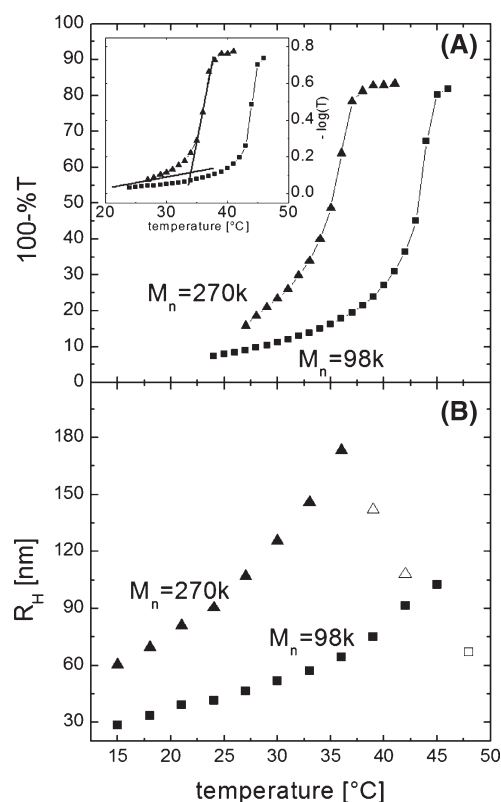


Figure 4. (A) Turbidity ($100 - \%T$) and (B) hydrodynamic size R_H as a function of temperature for the samples $C_p = 5$ g/L, $Y = 0.30$. Inset: $-\log(I)$ vs T showing means of defining T_ϕ . Open symbols in B are measurements for supernatant after settling of coacervate droplets at $T > T_\phi$.

$a = 1.0$, a plausible value if the complex is a highly extended chain; but at 35 °C, we obtain the unrealistically large $a = 1.7$, the limiting value of a for a rigid rod. This indicates that although the complexes may be intrapolymer at 15 °C, they must be aggregates thereof at higher temperature (obvious from their size) and that the degree of aggregation is larger for the higher MW polymer. For these aggregates, coacervation occurs about 10 °C lower than for the smaller ones obtained with PDADMAC $M_n = 98$ kDa. Regardless of this observation, the size of clusters at the point of incipient coacervation is substantially different for the two systems. This difference indicates that the apparent correlation between cluster size does not itself determine the coacervation point and T_ϕ , but rather, that both the size and T_ϕ arise from other causes.

Dilution experiments also show that there is no direct link between cluster size and T_ϕ . Figure 5A shows measurements of the hydrodynamic radius R_H as a function of T for samples with the same Y , polymer-to-surfactant stoichiometry, and salinity but varying polymer concentration C_p . The terminal data points in Figure 5 indicate the points of coacervation; hence, T_ϕ . We find that diluting the sample leads to smaller clusters size R_H (from ~ 110 nm to ~ 60 nm for polymer concentrations of 5 and 1.75 g/L at 27 °C). Despite the smaller cluster size, the coacervation domain expands to encompass lower temperatures (going from 37 to 25 °C). Hence, we find evidence for “self-suppression” in this system, meaning that the two-phase region actually contracts upon isoionic concentration.⁵⁴

It may seem puzzling that the coacervation would occur more easily (i.e., at lower T) in dilute samples than in concentrated ones. It

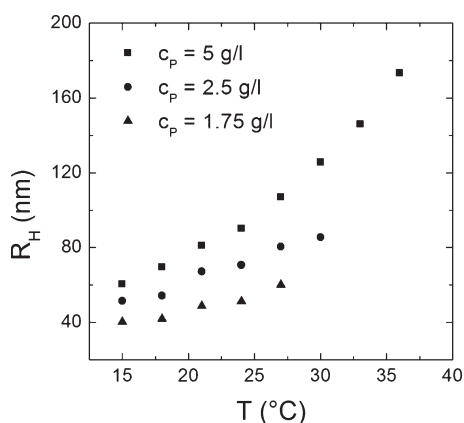


Figure 5. Hydrodynamic radius (R_H) as a function of temperature for PDADMAC/TX100-SDS with $M_n = 2.7 \times 10^5$; $Y = 0.30$. $C_p = 5, 2.5$, and 1.25 g/L; $T_\phi = 37, 31$, and 28 °C, respectively.

appears that cluster size by itself is not a trigger of coacervation. Instead, coacervation might be understood by considering the concentration of clusters and the interactions between them. If we consider the complexes as soft and rather complicated, self-assembled colloidal particles, then an increase in interparticle interactions or concentration could cause clustering and coacervation. By considering the interactions, we might explain why cluster size does not necessarily correlate with coacervation.

Cluster size and tendency to coacervate are correlated as shown in Figure 4, which suggests that they arise from a common origin. A reasonable common cause could be intercluster attraction. At the conditions for Y and bulk stoichiometry used here ($r = C_S/C_P$, the ratio of total surfactant and polymer concentrations), micelle surface charge density is too low to compensate for polymer charge ($Y = 0.38$ corresponds to a value of Y giving the lowest T_ϕ and also to complex charge neutrality).^{37,12,9} Therefore, the complexes have net positive charge. Long-range global repulsion among intrapolymer complexes can be compensated for by short-range attractions between micelles of one complex and polymers in another. This is facilitated by either polarization (the distribution of micelles within a complex becoming anisotropic) or disproportionation (transfer of SDS among micelles within a single complex, another source of charge anisotropy). It is reasonably evident that such effects are enhanced by increased MW. If we consider the complexes as soft colloidal particles, an increase in interparticle interactions simultaneously favors clustering and coacervation. The increase in cluster size with concentration does not necessarily lead to an enhancement of coacervation. It may be possible to explain the role of dilution by comparing the range of intercluster interaction to the mean distance between clusters. Considering the clusters as spheres of radius R_H , we can estimate the mean distance between their centers of mass as $d \sim R_H/\phi^{1/3}$, where ϕ is the volume fraction of clusters (the fraction of the sample volume that they comprise). The data of Figure 5 show that, R_H at coacervation is roughly proportional to polymer concentration, C_p . If we assume that ϕ is also proportional to C_p , then we find that $d \propto C_p^{2/3}$. Hence, a smaller C_p leads to smaller clusters, but the mean distance between them is also smaller; this proximity may lead to stronger interactions and a greater tendency to phase-separate.

In the proposed model, the interparticle interaction potential is a delicate balance of short-range and long-range forces, known

to cause formation of clusters of finite size and liquid–liquid phase separation⁴⁸ and is therefore consistent with the results of Figures 2–5. To the extent that long-range repulsions dominate, coacervation requires a larger entropic compensation, mainly arising from the release of counterions⁵⁵ that accompany more efficient ion pairing of micelles and polyelectrolytes. The role of entropy in this complex coacervation is clear not only from the temperature dependence but also from the lack of a favorable enthalpy during isothermal titration of PDADMAC with SDS/TX100 mixed micelles⁵⁶ and from DSC measurements passing through T_ϕ .³² The contribution of this favorable entropic term increases with temperature; thus, in the present system, deviations from $Y = 0.38$ (the condition for complex neutrality) systematically lead to larger values of T_ϕ .³⁷

Polydispersity and Disproportionation. Although splitting appears to accompany coacervation in Figure 1, there is less evidence of this for the low-MW polymer. The ambiguity of the splitting observation can be expressed in terms of two hypotheses: In the first, splitting involves a disproportionation driven by the favorable energy of coacervation, wherein a monomodal distribution of aggregates becomes bimodal to accommodate phase separation, with the smaller of the split-off species remaining in the dilute phase. In the second case, a pre-existing distribution of aggregates emerges prior to T_ϕ , some of them (here, the larger) more “coacervate-ready”. Since aggregation is promoted by charge neutrality^{12,9} and since the bulk charge stoichiometry ($[+]/[-]$) at these conditions is larger than 1, the formation of neutral complexes requires that some complexes contain either an above-average number of micelles or micelles with above-average SDS content. As noted above, this can involve a disproportionation or migration of surfactant, but could also be facilitated by pre-existing system heterogeneity.

To examine the role of polydispersity in the sample, we altered the most heterogeneous component of the system, the nonionic surfactant TX-100, which has a distribution of short polyethyleneoxide head groups. In some samples, we replaced TX-100 with the more homogeneous $C_{12}E_8$, with the results shown in Figure 6. Turbidimetric tracking of the phase change clearly shows it to be more abrupt than for TX-100, and a further reduction via “research grade” $C_{12}E_8$, confirms this trend. At the same time, we measured coacervate yield, which clearly shows that for TX-100, complexes or aggregates remaining in the dilute phase at some $T_1 > T_\phi$ will themselves coacervate at $T_2 > T_1$; comparison with data for $C_{12}E_8$ suggests that for this monodisperse nonionic surfactant, few remain in the dilute phase at $T_1 > T_\phi$.

We explain the data of Figure 6 with the following logical flow: (1) polydispersity of the nonionic leads to polydispersity of the mixed micelles; (2) polydispersity of the mixed micelles leads to polydispersity of complexes; (3) polydispersity of complexes/aggregates leads to a range of effective T_ϕ values (as suggested by Figure 6). We consider those hypotheses point-by-point. The distribution of n (the number of ethylene oxides within the headgroup) for the nonionic surfactant TX100 is likely to increase mixed-micelle polydispersity because micelles with different Y values can also contain nonionic surfactant molecules with n (the number of ethylene oxides within the headgroup) larger or smaller than the average $\bar{n} = 9.5$. In nonionic/anionic mixed-micelle systems, this polydispersity of nonionic surfactant leads to polydispersity of micelle size and microcomposition (y),

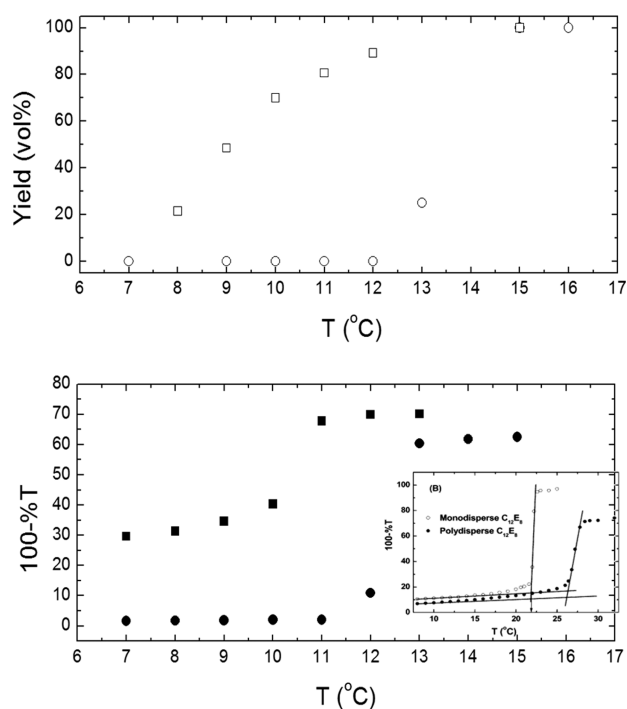


Figure 6. Effects of surfactant polydispersity. Effect of surfactant polydispersity on temperature dependence of coacervate yield (upper) or turbidity (lower). TX100 squares, $C_{12}E_8$ circles. Inset: mono- vs pauci-disperse $C_{12}E_8$.

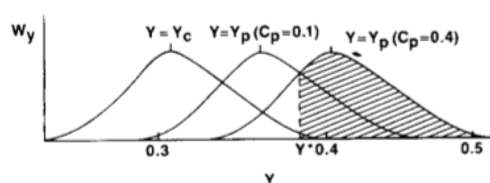


Figure 7. Hypothetical compositional distributions of mixed micelles at measured (average) values of Y corresponds to Y_c , Y_p ($C_p = 0.1$ wt %), and Y_p ($C_p = 0.4$ wt %). Y^* is the microscopic minimum value of Y required for micelle–polymer association, and the shaded area under the distribution curve is proportional to the concentration of associated micelles. From ref 59.

that is, charge^{57,58} as shown by capillary electrophoresis (CE) measurements for mixed micelles with either TX100 vs $C_{12}E_8$.

Previously, Oteri et al. suggested that the gradual increase in turbidity seen when PDADMAC+TX100 is titrated with SDS at $Y > Y_c$ (“type 1 titration”),⁵⁹ corresponds to a gradual increase in micelles with $y > y^*$ (i.e. “active micelles”) arising from a broad distribution of y (Figure 7). Indeed, the gradual increase seen for TX100 becomes abrupt when TX100 is replaced by $C_{12}E_8$; this corresponds to the more narrow mobility distribution for $C_{12}E_8$ /SDS micelles.⁵⁸ Further on the second point, it is found that complexes and aggregates are stable over a wide range in Y for the TX100-SDS/PDADMAC system, but only over a narrow range in Y for $C_{12}E_8$ -SDS; this suggests a broader distribution of complexes and aggregates for the former. Therefore, the replacement of polydisperse surfactant with monodisperse surfactant seems to reduce polydispersity among both micelles and soluble complexes.

Finally, we turn to the broadening of the temperature ramp of for TX-100/SDS in Figure 6. Fallon observed for this system a

continuous decrease in Y_c with temperature,⁶⁰ that is, a decrease in y^* , corresponding to an increase in the shaded area in Figure 7, which is used to visualize the fraction of the micelle distribution (with $y > y^*$) that binds to polymer. Raising the temperature thus increases this fraction of active micelles. If the compositional distribution is less broad (as for $C_{12}E_8$ /SDS), the fraction of active micelles increases much more rapidly because an increase in temperature causes y^* to decrease. This rapid increase in binding micelles with temperature is responsible for the dramatic narrowing of the temperature ramp curve in Figure 6 upon decrease in surfactant polydispersity.

The relationship between system heterogeneity and splitting of the size distribution is not obvious. The breadth of mobility distribution (distribution in y) for SDS-TX100 micelles, signifying a low energy barrier for compositional disproportionation, may have a parallel effect on complexes and aggregates. If the system strives for electroneutrality, complexes approach this by a combination of large n and small y , or vice versa. This could be reflected in a widening size distribution. Since $Y = 0.30$ as in Figures 1 and 2 is below the point of charge neutrality ($Y = 0.38$),³⁷ complexes are “undercharged” ($\bar{Z} > 0$), and coacervation can be promoted by the formation and transfer of more highly charged micelles to effectively neutralize those aggregates that may then coacervate. The compositional distribution for ionic/nonionic mixed micelles indicates a low energy barrier for micelle disproportionation, as supported by ref 61. The coexistence of intermacromolecular aggregates and single macromolecules of copolymer of *N*-vinylcaprolactam (VCA) and methacrylic acid (MA) with oppositely charged surfactant (cationic cetylpyridinium chloride, CPC) suggests the cooperative binding of CPC by copolymer chains, which leads to CPC disproportionation. In our system, the micelle facilitates disproportionation among complexes, enabling some of them to attain charge neutrality and, thus, cluster.

The coacervation of complexes at elevated temperature can arise from the favorable entropy of counterion release described above. Veis¹ also suggested that the less restricted motions of polymer chains within entangled coacervates, compared with those in complexes, could provide a favorable configurational entropy of coacervation, which may also be viewed as a form of surface tension. The disappearance of this effect when complexes are above the overlap concentration has been given as an origin of self-suppression of coacervation. Either counterion release or chain configurational relaxation could provide an entropy compensating for intercomplex repulsion. Alternatively, the exchange of micelles of different y among complexes to bring some of them to near neutrality. Such progressive intercomplex disproportionation, leading to the formation of micelles with $y > Y$ (in the present case), becomes progressively more difficult for the supernatant for which Y has become even smaller (complexes even more positive). An alternative hypothesis to coacervation of neutral complexes alone is intracomplex disproportionation, as proposed by Shklovskii,^{15,16} in which formation of dense regions of near macroion neutrality compensates for the incorporation of regions of nonzero macroion charge balance. Counterions, not considered by Shklovskii, would, of course, provide charge compensation for these regions, consistent with the findings of Cousin et al.⁵⁰ Although such disproportionation was proposed in ref 16 as a mechanism for formation of the condensed phase, the same driving forces could lead instead to larger aggregates, the formation of which benefits from the same enthalpic and entropic advantages as coacervation.

CONCLUSIONS

Temperature-induced liquid–liquid phase separation (coacervation) of polyelectrolyte–micelle complexes can be viewed as clustering of intricately hierarchical soft colloidal particles. It seems likely that complex particles interact through short-range attraction and long-range repulsion, the balance of which determines the length scales of their assemblies. As the critical temperature is approached, clusters grow and then split into larger and smaller aggregates. Although the appearance of large clusters and lower transition temperatures for complexes formed from a high-MW polyelectrolyte suggest a causal connection between cluster size and coacervation, the absence of such a correlation when cluster size is varied by isoionic dilution points instead toward the intercluster interaction potential as the primary causal property. The driving forces for coacervation are the entropy of counterion release, and the increase in intermacroionic charge complementarity, and are opposed by global intercomplex charge repulsion. Apart from net macroion charge stoichiometry, the effects of charge repulsion can be minimized by the migration or disproportionation of charged molecules or assemblies. That is facilitated by pre-existing polydispersity, demonstrated by the effects of introducing system heterogeneity through increased nonionic surfactant polydispersity.

AUTHOR INFORMATION

Corresponding Author

*E-mail: dubin@chem.umass.edu

ACKNOWLEDGMENT

Acknowledgment is made to the donors of The American Chemical Society Petroleum Research Fund for support of this research. We also acknowledge the facilities of NSF-supported UMass MRSEC on Polymers (DMR-0820506).

REFERENCES

- (1) Veis, A.; Aranyi, C. Phase Separation in Polyelectrolyte Systems 0.1. Complex Coacervates of Gelatin. *J. Phys. Chem.* **1960**, *64* (9), 1203–1210.
- (2) Strauss, G.; Gibson, S. A. Plant Phenolics As Cross-Linkers of Gelatin Gels and Gelatin-Based Coacervates for Use As Food Ingredients. *Food Hydrocolloid* **2004**, *18* (1), 81–89.
- (3) Mohanty, B.; Aswal, V. K.; Kohlbrecher, J.; Bohidar, H. B. Length Scale Hierarchy in Sol, Gel, and Coacervate Phases of Gelatin. *J. Polym. Sci. Polym. Phys.* **2006**, *44* (12), 1653–1665.
- (4) Kaibara, K.; Okazaki, T.; Bohidar, H. B.; Dubin, P. L. pH-Induced Coacervation in Complexes of Bovine Serum Albumin and Cationic Polyelectrolytes. *Biomacromolecules* **2000**, *1* (1), 100–107.
- (5) Antonov, M.; Mazzawi, M.; Dubin, P. L. Entering and Exiting the Protein–Polyelectrolyte Coacervate Phase via Nonmonotonic Salt Dependence of Critical Conditions. *Biomacromolecules* **2010**, *11* (1), 51–59.
- (6) Kayitmazer, A. B.; Strand, S. P.; Tribet, C.; Jaeger, W.; Dubin, P. L. Effect of Polyelectrolyte Structure on Protein–Polyelectrolyte Coacervates: Coacervates of Bovine Serum Albumin with Poly-(diallyldimethylammonium chloride) versus Chitosan. *Biomacromolecules* **2007**, *8* (11), 3568–3577.
- (7) Liu, S. H.; Cao, Y. L.; Ghosh, S.; Rousseau, D.; Low, N. H.; Nickerson, M. T. Intermolecular Interactions during Complex Coacervation of Pea Protein Isolate and Gum Arabic. *J. Agric. Food Chem.* **2010**, *58* (1), 552–556.
- (8) Leisner, D.; Imae, T. Interpolyelectrolyte Complex and Coacervation Formation of Poly(glutamic acid) with a Dendrimer Studied by Light Scattering and SAXS. *J. Phys. Chem. B* **2003**, *107* (32), 8078–8087.
- (9) Wang, Y. L.; Kimura, K.; Dubin, P. L.; Jaeger, W. Polyelectrolyte–Micelle Coacervation: Effects of Micelle Surface Charge Density, Polymer Molecular Weight, and Polymer/Surfactant Ratio. *Macromolecules* **2000**, *33* (9), 3324–3331.
- (10) Feng, X. H.; Dubin, P. L.; Zhang, H. W.; Kirton, G. F.; Bahadur, P.; Parotte, J. Critical Conditions for Binding of Dimethyldodecylamine Oxide Micelles to Polyanions of Variable Charge Density. *Macromolecules* **2001**, *34* (18), 6373–6379.
- (11) Li, Y. J.; Dubin, P. L.; Dautzenberg, H.; Luck, U.; Hartmann, J.; Tuzar, Z. Dependence of Structure of Polyelectrolyte/Micelle Complexes upon Polyelectrolyte Chain-Length and Micelle Size. *Macromolecules* **1995**, *28* (20), 6795–6798.
- (12) Wang, Y. L.; Kimura, K.; Huang, Q. R.; Dubin, P. L.; Jaeger, W. Effects of Salt on Polyelectrolyte–Micelle Coacervation. *Macromolecules* **1999**, *32* (21), 7128–7134.
- (13) Evers, O. A.; Fleer, G. J.; Scheutjens, J. M. H. M.; Lyklema, J. Adsorption of Weak Polyelectrolytes from Aqueous Solution. *J. Colloid Interface Sci.* **1986**, *111* (2), 446–454.
- (14) Vongeler, F.; Muthukumar, M. Adsorption of Polyelectrolytes onto Curved Surfaces. *J. Chem. Phys.* **1994**, *100* (10), 7796–7803.
- (15) Nguyen, T. T.; Shklovskii, B. I. Complexation of DNA with Positive Spheres: Phase Diagram of Charge Inversion and Reentrant Condensation. *J. Chem. Phys.* **2001**, *115* (15), 7298–7308.
- (16) Zhang, R.; Shklovskii, B. T. Phase Diagram of Solution of Oppositely Charged Polyelectrolytes. *Physica A* **2005**, *352* (1), 216–238.
- (17) Leclercq, S.; Harlander, K. R.; Reineccius, G. A. Formation and Characterization of Microcapsules by Complex Coacervation with Liquid or Solid Aroma Cores. *Flavour Frag. J.* **2009**, *24* (1), 17–24.
- (18) Clarke, A. W.; Arnsperg, E. C.; Mithieux, S. M.; Korkmaz, E.; Braet, F.; Weiss, A. S. Tropoelastin Massively Associates during Coacervation to Form Quantized Protein Spheres. *Biochemistry* **2006**, *45* (33), 9989–9996.
- (19) Gruber, J. V. Polyquaternium-10: Cornerstone of a Personal Care Revolution. *J. Cosmet. Sci.* **2009**, *60* (3), 385–386.
- (20) Xia, J. L.; Mattison, K.; Romano, V.; Dubin, P. L.; Muhoberac, B. B. Complexation of Trypsin and Alcohol Dehydrogenase with Poly-(diallyldimethylammonium chloride). *Biopolymers* **1997**, *41* (4), 359–365.
- (21) Benichou, A.; Aserin, A.; Garti, N. Protein–Polysaccharide Interactions for Stabilization of Food Emulsions. *J. Dispers. Sci. Technol.* **2002**, *23* (1–3), 93–123.
- (22) de Kruif, C. G.; Weinbreck, F.; de Vries, R. Complex Coacervation of Proteins and Anionic Polysaccharides. *Curr. Opin. Colloid Interface Sci.* **2004**, *9* (5), 340–349.
- (23) Turgeon, S. L.; Schmitt, C.; Sanchez, C. Protein–Polysaccharide Complexes and Coacervates. *Curr. Opin. Colloid Interface Sci.* **2007**, *12* (4–5), 166–178.
- (24) Burgess, D. J.; Ponsart, S. β -Glucuronidase Activity Following Complex Coacervation and Spray Drying Microencapsulation. *J. Microencapsul.* **1998**, *15* (5), 569–579.
- (25) Stevens, M. J.; Steren, R. E.; Hlady, V.; Stewart, R. J. Multiscale Structure of the Underwater Adhesive of *Phragmatopoma californica*: A Nanostructured Latex with a Steep Microporosity Gradient. *Langmuir* **2007**, *23* (9), 5045–5049.
- (26) Michaeli, I.; Overbeek, J. T. G.; Voorn, M. J. Phase Separation of Polyelectrolyte Solutions. *J. Polym. Sci.* **1957**, *23* (103), 443–450.
- (27) Veis, A.; Bodor, E.; Mussell, S. Molecular Weight Fractionation and Self-Suppression of Complex Coacervation. *Biopolymers* **1967**, *5* (1), 37.
- (28) Sato, H.; Nakajima, A. Complex Coacervation in Sulfated Polyvinyl Alcohol–Aminoacetylated Polyvinyl Alcohol System 0.2. Formation of Coacervate Droplets. *Colloid Polym. Sci.* **1974**, *252* (11), 944–948.
- (29) Sperber, B. L. H. M.; Schols, H. A.; Stuart, M. A. C.; Norde, W.; Voragen, A. G. J. Influence of the Overall Charge and Local Charge Density of Pectin on the Complex Formation between Pectin and β -Lactoglobulin. *Food Hydrocolloid* **2009**, *23* (3), 765–772.
- (30) Schmitt, C.; Sanchez, C.; Thomas, F.; Hardy, J. Complex Coacervation between β -Lactoglobulin and Acacia Gum in Aqueous Medium (vol 13, pg 483, 1999). *Food Hydrocolloid* **2000**, *14* (6), 617–617.

- (31) Espinosa-Andrews, H.; Sandoval-Castilla, O.; Vazquez-Torres, H.; Vernon-Carter, E. J.; Lobato-Calleros, C. Determination of the Gum Arabic–Chitosan Interactions by Fourier Transform Infrared Spectroscopy and Characterization of the Microstructure and Rheological Features of Their Coacervates. *Carbohydr. Polym.* **2010**, *79* (3), 541–546.
- (32) Dubin, P. L.; Li, Y. J.; Jaeger, W. Mesophase Separation in Polyelectrolyte-Mixed Micelle Coacervates. *Langmuir* **2008**, *24* (9), 4544–4549.
- (33) Chodankar, S.; Aswal, V. K.; Kohlbrecher, J.; Vavrin, R.; Wagh, A. G., Structural Study of Coacervation in Protein–Polyelectrolyte Complexes. *Phys. Rev. E* **2008**, *78* (3), 031913.
- (34) Kayitmazer, A. B.; Bohidar, H. B.; Mattison, K. W.; Bose, A.; Sarkar, J.; Hashidzume, A.; Russo, P. S.; Jaeger, W.; Dubin, P. L. Mesophase Separation and Probe Dynamics in Protein–Polyelectrolyte Coacervates. *Soft Matter* **2007**, *3* (8), 1064–1076.
- (35) Bohidar, H.; Dubin, P. L.; Majhi, P. R.; Tribet, C.; Jaeger, W. Effects of Protein–Polyelectrolyte Affinity and Polyelectrolyte Molecular Weight on Dynamic Properties of Bovine Serum Albumin–Poly(diallyldimethylammonium chloride) Coacervates. *Biomacromolecules* **2005**, *6* (3), 1573–1585.
- (36) Liberatore, M. W.; Wyatt, N. B.; Henry, M.; Dubin, P. L.; Foun, E. Shear-Induced Phase Separation in Polyelectrolyte/Mixed Micelle Coacervates. *Langmuir* **2009**, *25* (23), 13376–13383.
- (37) Kumar, A.; Dubin, P. L.; Hernon, M. J.; Li, Y. J.; Jaeger, W. Temperature-Dependent Phase Behavior of Polyelectrolyte–Mixed Micelle Systems. *J. Phys. Chem. B* **2007**, *111* (29), 8468–8476.
- (38) Boral, S.; Bohidar, H. B. Effect of Ionic Strength on Surface-Selective Patch Binding-Induced Phase Separation and Coacervation in Similarly Charged Gelatin–Agar Molecular Systems. *J. Phys. Chem. B* **2010**, *114* (37), 12027–12035.
- (39) Wang, X.; Wang, Y. W.; Ruengruglikit, C.; Huang, Q. Effects of Salt Concentration on Formation and Dissociation of β -Lactoglobulin/Pectin Complexes. *J. Agric. Food Chem.* **2007**, *55* (25), 10432–10436.
- (40) Nguyen, T. T.; Rouzina, I.; Shklovskii, B. I. Reentrant Condensation of DNA Induced by Multivalent Counterions. *J. Chem. Phys.* **2000**, *112* (5), 2562–2568.
- (41) Poon, W. C. K. The Physics of a Model Colloid–Polymer Mixture. *J. Phys.: Condens. Matter* **2002**, *14* (33), R859–R880.
- (42) Groenewold, J.; Kegel, W. K. Anomalous Large Equilibrium Clusters of Colloids. *J. Phys. Chem. B* **2001**, *105* (47), 11702–11709.
- (43) Lu, P. J.; Conrad, J. C.; Wyss, H. M.; Schofield, A. B.; Weitz, D. A. Fluids of Clusters in Attractive Colloids. *Phys. Rev. Lett.* **2006**, *96* (2), 028306.
- (44) Sedgwick, H.; Egelhaaf, S. U.; Poon, W. C. K. Clusters and Gels in Systems of Sticky Particles. *J. Phys.: Condens. Matter* **2004**, *16* (42), S4913–S4922.
- (45) Stradner, A.; Sedgwick, H.; Cardinaux, F.; Poon, W. C. K.; Egelhaaf, S. U.; Schurtenberger, P. Equilibrium Cluster Formation in Concentrated Protein Solutions and Colloids. *Nature* **2004**, *432* (7016), 492–495.
- (46) Campbell, A. I.; Anderson, V. J.; van Duijneveldt, J. S.; Bartlett, P. Dynamical Arrest in Attractive Colloids: The Effect of Long-Range Repulsion. *Phys. Rev. Lett.* **2005**, *94* (20), 208301.
- (47) Gibson, H. M.; Wilding, N. B. Metastable Liquid–Liquid Coexistence and Density Anomalies in a Core-Softened Fluid. *Phys. Rev. E* **2006**, *73* (6), 061507.
- (48) Archer, A. J.; Wilding, N. B. Phase Behavior of a Fluid with Competing Attractive and Repulsive Interactions. *Phys. Rev. E* **2007**, *76* (3), 031501.
- (49) Schmidt, I.; Cousin, F.; Huchon, C.; Boue, F.; Axelos, M. A. V. Spatial Structure and Composition of Polysaccharide–Protein Complexes from Small Angle Neutron Scattering. *Biomacromolecules* **2009**, *10* (6), 1346–1357.
- (50) Cousin, F.; Gummel, J.; Clemens, D.; Grillo, I.; Boue, F. Multiple Scale Reorganization of Electrostatic Complexes of Poly(styrenesulfonate) and Lysozyme. *Langmuir* **2010**, *26* (10), 7078–7085.
- (51) Gummel, J.; Boue, F.; Clemens, D.; Cousin, F. Finite Size and Inner Structure Controlled by Electrostatic Screening in Globular Complexes of Proteins and Polyelectrolytes. *Soft Matter* **2008**, *4* (8), 1653–1664.
- (52) Hahn, M.; Jaeger, W. Kinetics of the Free-Radical Polymerization of Dimethyl Diallyl Ammonium Chloride, 0.5. Kinetic Model with Persulfate as Initiator. *Angew. Makromol. Chem.* **1992**, *198*, 165–178.
- (53) Provencher, S. W. Contin—a General-Purpose Constrained Regularization Program for Inverting Noisy Linear Algebraic and Integral-Equations. *Comput. Phys. Commun.* **1982**, *27* (3), 229–242.
- (54) Li, Y. J.; Dubin, P. L.; Havel, H. A.; Edwards, S. L.; Dautzenberg, H. Electrophoretic Light-Scattering, Dynamic Light-Scattering, and Turbidimetry Studies of the Effect of Polymer Concentration on Complex-Formation between Polyelectrolyte and Oppositely Charged Mixed Micelles. *Macromolecules* **1995**, *28* (9), 3098–3102.
- (55) Ball, V.; Winterhalter, M.; Schwinte, P.; Lavalle, P.; Voegel, J. C.; Schaaf, P. Complexation Mechanism of Bovine Serum Albumin and Poly(allylamine hydrochloride). *J. Phys. Chem. B* **2002**, *106* (9), 2357–2364.
- (56) Rigsbee, D. R.; Dubin, P. L. Microcalorimetry of Polyelectrolyte Micelle Interactions. *Langmuir* **1996**, *12* (7), 1928–1929.
- (57) Zhang, H.; Li, Y.; Dubin, P.; Kato, T. Effect of EO Chain Length of Dodecanol Ethoxylates (C(12)E(n)) on the Complexation of C-(12)E(n)/SDS Mixed Micelles with an Oppositely Charged Polyelectrolyte. *J. Colloid Interface Sci.* **1996**, *183* (2), 546–551.
- (58) Zhang, B.; Kirton, G. F.; Dubin, P. L. Compositional Heterogeneity in Anionic/Nonionic Mixed Micelles Observed by Frontal Analysis Continuous Capillary Electrophoresis. *Langmuir* **2002**, *18* (12), 4605–4609.
- (59) Dubin, P. L.; Oteri, R. Association of Poly-Electrolytes with Oppositely Charged Mixed Micelles. *J. Colloid Interface Sci.* **1983**, *95* (2), 453–461.
- (60) Fallon, M. A. M.S. Thesis, Purdue University, West Lafayette, IN, 1988.
- (61) Makhaeva, E. E.; Tenhu, H.; Khokhlov, A. R. Behavior of Poly(*N*-vinylcaprolactam-co-methacrylic acid) Macromolecules in Aqueous Solution: Interplay between Coulombic and Hydrophobic Interaction. *Macromolecules* **2002**, *35* (5), 1870–1876.